

Microresonator and Laser Parameter Definition via Self-Injection Locking

Artem E. Shitikov^{1,2,*}, Oleg V. Benderov^{1,3}, Nikita M. Kondratiev¹, Valery E. Lobanov¹, Alexander V. Rodin^{1,3}, and Igor A. Bilenko^{1,2}

¹ Russian Quantum Center, Skolkovo 143026, Russia

² Faculty of Physics, Lomonosov Moscow State University, Moscow 119991, Russia

³ Moscow Institute of Physics and Technology, Dolgoprudny 141701, Russia



(Received 29 July 2020; revised 9 October 2020; accepted 19 November 2020; published 15 December 2020)

Self-injection locking to a high-quality-factor microresonator is a key component of various up-to-date photonic applications, including compact narrow-linewidth lasers and microcomb sources. For optimal construction of such devices, it is necessary to know the parameters of the locking mode, which is a challenging task. We experimentally develop and verify an original technique based on the fundamentals of the self-injection locking effect, which allows determining the key parameters of the mode of the microresonator (quality factor, vertical index) as well as the laser diode parameters. We demonstrate that this method can be used in the spectral ranges where conventional methods are not applicable, for example, in the mid-IR. We stabilize a $2.64\ \mu\text{m}$ laser diode by a high- Q whispering gallery mode microresonator made of crystalline silicon. Using the elaborated technique, the quality factor of the microresonator is determined to be 5×10^8 .

DOI: [10.1103/PhysRevApplied.14.064047](https://doi.org/10.1103/PhysRevApplied.14.064047)

I. INTRODUCTION

The effect of self-injection locking (SIL) has been utilized for many years in radiophysics and microwave electronics to stabilize the devices and to increase their spectral purity [1–7]. For more than the last three decades, it has also been studied and actively applied in optics and laser physics [8–19]. The most interesting results were demonstrated with whispering gallery mode (WGM) microresonators [20–30], combining a large quality factor in a wide spectral range with small size and low environmental sensitivity. Nowadays, this effect is a key ingredient of various up-to-date photonic applications. The Rayleigh backscattering in optical microresonators [31] provides a passive frequency-selective fast optical feedback to the laser diode, resulting in significant laser phase noise suppression and linewidth reduction. Recent research has demonstrated passive stabilization of single-frequency [32–37] or even multifrequency [38–41] semiconductor lasers to subkilohertz linewidths with WGM microresonators in different spectral ranges, from UV to mid-IR. Moreover, it was shown that such stabilized laser diodes can be used as a pump source for the generation of the microresonator-based frequency combs [40]. High attainable Q factors and the small mode volume of the WGM allows decreasing the soliton generation power threshold to several microwatts, which opens the way to compact energy-efficient devices.

The development of such compact microcomb sources is one of the hottest topics of modern photonics that attracts researchers worldwide [40,42–46]. Such devices are of paramount importance in numerous areas of modern science and technology, such as coherent communication [47,48], ultrafast optical ranging and LIDARs [49–51], high-precision spectroscopy [52,53], astrophysics [54,55], low-noise microwave synthesis [35], and optical clocks [56,57].

Constructing such microresonator-based devices operating in the SIL regime, one may face a challenging problem of the accurate determination of the locking microresonator mode parameters. Its quality factor is a crucial parameter that determines the effectiveness of SIL and overall device performance, since it determines the resulting linewidth of the laser source defining the stabilization coefficient [58] and the threshold of the nonlinear effects [59]. The highest Q factor can be achieved in WGM crystalline resonators (up to 10^{11} [23]), and the application of prism couplers made devices with such resonators work perfectly and robustly. There are several well-known ways to measure the quality factor: the full width at half maximum (FWHM) of the resonance curve measurement, the ringdown method based on the recording of free oscillations after pulsed excitation, and evaluation from the linewidth dependence on the microresonator loading [60]. However, in the SIL regime, such methods are mostly non-applicable. First, they require an optical isolator between the laser and the microresonator, which leads to the need

*Shitikov@physics.msu.ru

for the disassembly and subsequent assembly of the device or the setup. Second, a determination of the particular WGM that is used for SIL can be a challenging task in the overmoded resonators. Also, in some spectral ranges, the use of these methods requires the availability of hard-to-find and expensive instruments.

In our work, we analyze in detail the manifestations of SIL for different types and parameters of the microresonator modes and show that SIL can be used as an effective diagnostic tool. We find that SIL transmission curves depend on the microresonator Q factor in a fashion that allows extracting it directly from the locking range measurement, which makes it unnecessary to measure the microresonator quality factor from the frequency or time response of the unlocked resonator. We develop an original method based on the measurement of the SIL bandwidth as a function of the gap between the coupling prism and the microresonator. The possibility of varying the coupling rate by changing the size of the gap gives a useful degree of freedom (inaccessible in the case of Fabry-Pérot cavities). The technique also offers a unique opportunity for determining the intrinsic quality factor of the exact WGM used in the SIL regime. Besides, the developed method allows one to determine the vertical index of the selected mode and provides information about a laser diode parameter—the output beam coupling rate—which is of particular importance for accurate SIL modeling and microresonator-based device construction. This technique is based on the fundamentals of SIL and is valid for any wavelength and microresonator and is verified at 1550 nm for MgF_2 by the conventional well-adopted ringdown method. We also compare the elaborated technique with the alternative techniques and show that it is especially useful for the WGM Q factor determination in specific wavelength ranges where it is difficult to do using conventional methods due to the lack of necessary devices (high-speed detectors, narrow-linewidth lasers).

We successfully apply the technique for silicon resonators in the mid-IR band, avoiding the need to use an expensive narrow-linewidth tunable laser. We demonstrate SIL of a laser diode to a WGM microresonator made of crystalline silicon at a wavelength of $2.6 \mu\text{m}$, and characterize the effect using the abovementioned technique. The Q factor of the WGM is up to 0.5×10^9 , and the locking width exceeds 0.6 GHz. The mid-IR laser diodes' significant stabilization seems to be very interesting because there is a shortage of affordable, narrow-linewidth laser sources in the enormous range from 2 to 20 μm . Commonly used optical parametric oscillators and quantum cascaded lasers with distributed feedback are rather expensive and hard-to-obtain products. Sub-kilohertz lasers have great potential in the mid-IR range since it covers the molecular fingerprint region important for high-resolution gas spectroscopy [61], biosensing [62], and even fundamental constant measurements [63]. It is also promising for free-space optical communication due to better performance than the near-IR light in fog conditions because it suffers less from atmospheric turbulence [64]. For optical communication, a narrow-linewidth laser source allows high-order modulation to increase the bit rate [65]. The demonstration of the high-quality factor in a silicon microresonator in the mid-IR is also a new step in silicon photonics. The high nonlinear refractive index, $n_2 = 4.5 \times 10^{-18} \text{ m}^2/\text{W}$ [66], combined with the absence of the multiphonon absorption up to 8 μm [67] and two-photon absorption from 2.3 μm [66] opens up a new perspective for silicon in the mid-IR since the quality factor of the commonly used fluoride WGM reference cavities can be limited by the multiphonon absorption [29].

II. SIL-BASED MEASUREMENT TECHNIQUE

We consider a typical microresonator experimental setup (see Fig. 1) with piezo elements to control the

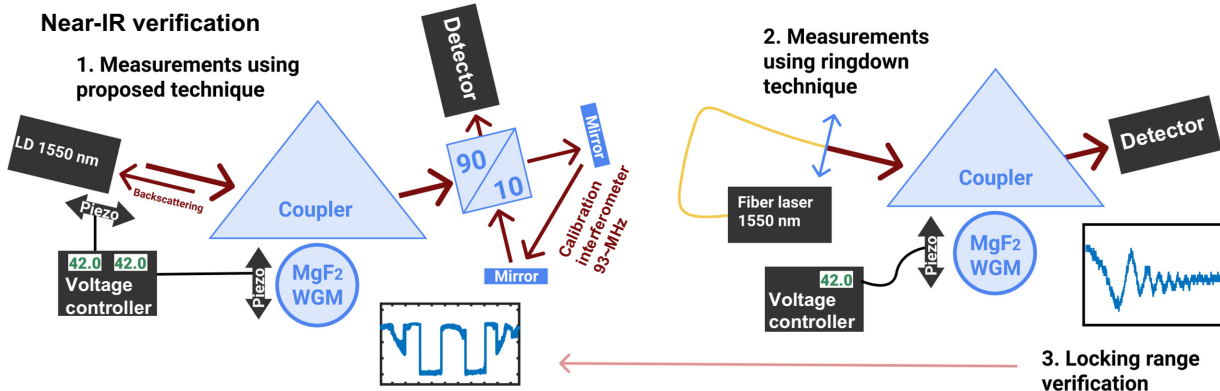


FIG. 1. Experimental setups in the near-IR. First, we measure the dependence of the resonance width on the gap value between the microresonator and the coupler. Second, we measure the Q factor of that mode by the ringdown method. Finally, we verify that the Q factor conserves during measurements by measuring the resonance width another time.

microresonator coupling and the laser-microresonator distance. We study different types of dependencies of the transmitted light intensity from the laser diode current (LI curves), observed in experiments with a photodiode, which corresponds to a frequency scan of a laser diode. In the case of SIL the LI curve shape varies with the phase of the backscattering wave ψ_0 gained while traveling from the laser to the microresonator and back. The locking phase ψ_0 strongly affects the laser stabilization and can be controlled by adjusting the distance between the laser diode and WGM microresonator. In our experiments the locking phase ψ_0 is precisely controlled by a piezo element (see Fig. 1). Calculated dependencies of the transmitted power on the laser detuning from the WGM frequency are shown in Fig. 2. A free resonance is observed in the absence of backscattering (black dotted line in Fig. 2) and a locked resonance appears when the backscattering causes SIL (blue dashed line in Fig. 2). In the self-injection locking regime, one may determine the locking range, which is the bandwidth on the LI curve where the frequency change is suppressed by SIL. At locking phases $\psi_0 \in [-\pi/2; \pi/2]$, the locking range is bounded by sharp edges. For non-even locking phases ($\psi_0 \neq \pi n$), the shape of the LI curves during the forward and backward frequency scans are different, which can be seen in the experiment. This means that we need both scans to capture the whole locking band correctly. The theoretical predictions are shown in Fig. 2 with solid lines plus highlighted with triangles. The sum of the forward locking range (FLR), measured on the forward scan, and backward locking range (BLR), measured on the backward scan, is connected with the locking range $\delta\omega_{\text{lock}}$ as $\text{FLR} + \text{BLR} = \delta\omega_{\text{lock}} + \delta\omega_{\text{in}}$ (see Fig. 2). The FLR-BLR overlap or the inner band $\delta\omega_{\text{in}}$ is significant only for a low intrinsic quality factor Q_{int} or for an overcoupled microresonator.

We note that in the locked state the width of the locking range can be naturally defined using the sharp jumps of

the curve. Self-injection locking theory predicts that this width depends on the loaded quality factor of the locking WGM Q_m ($1/Q_m = 1/Q_{\text{int}} + 1/Q_{\text{coupl}}$, where Q_{coupl} represents losses added by the coupler that extracts light from the resonator) [58]. Using this theory, we propose a technique, based on measuring FLR + BLR dependence on a gap between the cavity and the coupler, which provides information on the locking mode's intrinsic quality factor Q_{int} and its vertical index. Knowing Q_{int} one may estimate Q_m for every gap value.

Using the expression for the stationary tuning curve for the zero locking phase $\psi_0 = 0$ [58], one may obtain the following expressions for the total locking range width $\delta\omega_{\text{lock}}$ and for the width of the inner band $\delta\omega_{\text{in}}$ in the case of the zero locking phase:

$$\delta\omega_{\text{lock}} \approx 3\sqrt{3}\gamma \frac{\kappa_{\text{mc}}}{\kappa_m^2} \bar{\kappa}_{\text{do}} + \frac{\sqrt{3}}{3} \kappa_m, \quad (1)$$

$$\delta\omega_{\text{in}} \approx 8\sqrt[4]{\frac{\kappa_{\text{mc}}\kappa_m\gamma\bar{\kappa}_{\text{do}}}{27}}. \quad (2)$$

Here, γ is the forward-backward wave coupling rate, $\bar{\kappa}_{\text{do}}$ is the laser's effective (hot) output beam coupling rate, and $\kappa_m = \kappa_{\text{mc}} + \kappa_{\text{mi}}$ is the microresonator's mode decay rate, where κ_{mi} is determined by the intrinsic losses and κ_{mc} is determined by the coupling losses. The corresponding values of the loaded and intrinsic quality factor are defined as $Q_m = \omega/\kappa_m$, $Q_{\text{int}} = \omega/\kappa_{\text{mi}}$. One can load a microresonator by moving it closer to the coupler. The microresonator is called overcoupled when κ_{mc} is larger than κ_{mi} and undercoupled when κ_{mi} is larger than κ_{mc} . When κ_{mi} equals κ_{mc} , the coupling is called critical. It should be noted that Eqs. (1) and (2) provide good estimations for the widths of the discussed bands for the locking phases $\psi_0 \in [-\pi/2; \pi/2]$. In an experiment the locking phase close to

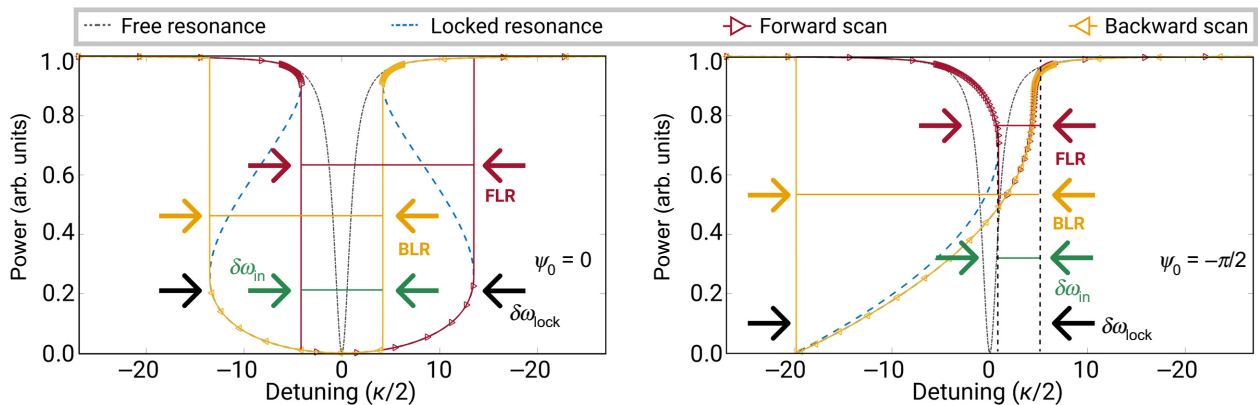


FIG. 2. Calculated normalized transmitted power dependence on the detuning of the laser frequency from the WGM frequency for the different locking phases. The sum of the forward and backward locking ranges is measured in the experiments. It is a good approximation of the total locking range $\delta\omega_{\text{lock}}$ in the case of a high Q factor, when the inner overlap band $\delta\omega_{\text{in}}$ is negligible.

zero is the most desirable due to the best performance [68]. The second term in Eq. (1) becomes a significant part of the locking range only in close proximity of the coupler, where κ_{mc} is large. However, the locking range (1) is actually determined at a level greater than half of the maximum intensity and, thus, does not correspond to the FWHM that is usually used for the Lorentzian-like curve characterization and equals the resonator loss rate. During loading, Q_m decreases and at some point the sharp edges of the locking band are blurred, upon which the FWHM should be measured to characterize the mode. Using the tuning curve expression from Ref. [58], one can obtain the following expression for the FWHM in the SIL regime:

$$\delta\omega_{FWHM} = 4\gamma \frac{\kappa_{mc}}{\kappa_m^2} \bar{\kappa}_{do} + \kappa_m. \quad (3)$$

It can be seen that $\delta\omega_{FWHM}$ is smaller than the full locking range $\delta\omega_{lock}$ for high values of the intrinsic quality factor and cannot be observed as it is hidden behind the LI curve jumps, so Eq. (1) should be used to estimate the locking width. If the locking width is reduced, a transition from the “hard” (with jumps) to “soft” (smooth curve) regime occurs. The transition point occurs when all the three widths are equal to the double unlocked microresonator linewidth: $\delta\omega_{lock} = \delta\omega_{in} = \delta\omega_{FWHM} = 2\kappa_m$. After this transition occurs, $\delta\omega_{FWHM}$ becomes larger than the full locking width and the curve no longer has any jumps [Eq. (2) becomes meaningless], making the use of $\delta\omega_{FWHM}$ reasonable for the width estimations. When the first term of Eq. (3) is much smaller than the second term, $\delta\omega_{FWHM}$ is equal to the microresonator total loss rate κ_m , the curve shape becomes Lorentzian, and SIL is totally switched off.

Analyzing the derivative of Eq. (1) with respect to the microresonator coupling rate κ_{mc} , one sees that its maximum takes place at the critical coupling $\kappa_{mi} = \kappa_{mc}$. Knowing κ_{mc} at the maximum locking range one would also know κ_{mi} . At the same time, κ_{mc} can be evaluated from the value of the gap between the microresonator and the coupler d [69]:

$$\kappa_{mc} \approx \frac{\omega}{2} \left(\frac{n^2 - 1}{n} k \right)^{-3/2} \exp\{(-2kd\sqrt{n^2 - 1})\} \times \begin{cases} 1/\sqrt{\pi/(1 + \sqrt{n^2 - 1})}, & p = 0, \\ 1/(\sqrt{2}\pi\sqrt{p}), & p > 0. \end{cases} \quad (4)$$

Here both the refractive indices of the coupler and the microresonator are assumed to be equal to n , ω is the pump frequency, a is the radius of the microresonator, $k = \omega/c$, and p is the vertical index of the mode. It is assumed that the refractive index of the coupler is approximately equal to the refractive index of the microresonator, which is exactly true in our case of a Si resonator with a silicon hemisphere coupler and quite acceptable for MgF₂.

TABLE I. Coupling rate κ_{mc} of the WGM at zero gap in megahertz.

	<i>p</i>					
	0	1	2	3	4	5
MgF ₂ 1550 nm	159	52	37	30	26	23
Si 2639 nm	90	14	10	8	7	6

with a glass prism. Thus, the position of the extremum of the curve describing the dependence of the locking range width (or FLR + BLR in our experiments) on the gap between the microresonator and coupling element provides us with information about the locking mode’s critical coupling. The accuracy of the technique depends on the accuracy of the maximum of the locking width position corresponding to the coupler position measurements. Note that, according to Ref. [68], critical coupling provides the optimal laser stabilization in most cases, and thus the obtained information can also be used for the fine tuning of SIL-based devices using the same piezo element.

It is worth noting that, according to Eq. (4), the coupling-related linewidth of the microresonator at zero gap in the case of high Q_{int} is mostly determined by the vertical index p of the WGM (see Table I for a 2 mm radius for MgF₂ at 1550 nm and a 1.25 mm radius for Si at 2639 nm). Thus, knowing κ_m at zero gap one can evaluate the vertical index of the mode from Eq. (4). The difference between linewidth due to loading at zero gap $\kappa_{mc}(d = 0)$ for microresonators made of MgF₂ and Si is maximum for $p = 0$ and $p = 1$, decreasing with increasing p .

Summarizing, to determine a WGM’s parameters in the SIL regime, one needs to measure the dependence of the sum of FLR and BLR on the gap between the coupler and microresonator. Also, it is necessary to monitor the change of the LI curve shape. There can be two cases: the first case in which the “hard” SIL regime with sharp LI curve edges is maintained up to the zero gap, and the second case in which the “soft” SIL regime with smooth edges appears in the proximity of the coupler.

The fit process of the measured dependence is carried out by the brute force method. In the first case we start with selecting Q_{int} to match the position of the experimental curve maximum with Eqs. (1) and (2) using Eq. (4) for several p values. Then we adjust $\gamma\bar{\kappa}_{do}$ to fit FLR + BLR at critical coupling and choose the best variant at the zero point over the p indices. In the second case the fit process is almost the same but the p index can be estimated from the data at zero gap using Table I. Then we select Q_{int} to match the maximum of the experimental curve with Eqs. (1) and (2) using Eq. (4). Then, we adjust $\gamma\bar{\kappa}_{do}$ in order to match the locking range value at the maximum point. The part of the measured dependence related to the “soft” regime should be fitted with $2\delta\omega_{FWHM}$ from Eqs. (3) and (4) using the parameters determined in previous steps,

and good coincidence indicates the correct choice of the parameters (p in particular). The uncertainty of the measurements can be added according to the piezo element voltage controller step.

The only alternative for determining the Q factor in the SIL regime is a technique based on resonance depth analysis [60]. This technique is similar to the coupling rate exponential fitting (4), but we use the resonator power transmittance curve. Firstly, the resonance depth measurements are sensitive to the coupling of all light into the detector (which can be challenging in many cases) and different detector noises. Secondly, it is necessary to emphasize that it is vital to determine the vertical index of the mode as described above to calculate the Q factor correctly. Finally, it is very natural to measure the locking range in the SIL regime. It can be measured very accurately and is not demanding for the equipment parameters. For a rough estimate of Q_{int} , one does not need to measure dozens of points; it is sufficient to determine the zero-gap point for the vertical index p determination, and the critical coupling point to relate the coupling to the intrinsic loss. FLR + BLR at these points provides enough information to completely fit with Eqs. (1), (3), and (4).

Once the locking range for the given resonator and coupling rate is obtained, it can be used to characterize the laser diode. In the case of the high- Q WGM the second term in Eq. (1) is negligible and, for the effective (hot) output beam coupling rate $\bar{\kappa}_{\text{do}}$, from Eq. (1), one obtains

$$\bar{\kappa}_{\text{do}} = \frac{1}{3\sqrt{3}} \frac{\delta\omega_{\text{lock}}\kappa_m^2}{\gamma\kappa_{\text{mc}}} = \frac{4}{3\sqrt{3}} \frac{\delta\omega_{\text{lock}}}{\Gamma_m}, \quad (5)$$

where $\Gamma_m = 4(\gamma\kappa_{\text{mc}}/\kappa_m^2)$ is the amplitude reflection coefficient from the WGM cavity at resonance [58], which can be measured experimentally. On the other hand, $\bar{\kappa}_{\text{do}} = (T_o^2/\tau_d R_e R_o^2)\sqrt{1+\alpha_g^2}$, where R_o and R_e are the amplitude reflection coefficients of the output and end laser mirrors, $T_o = \sqrt{1 - R_o^2}$ is the output amplitude transmission coefficient, τ_d is the round-trip time of a laser diode, and α_g is the Henry factor, which allows us to take into account the refractive index changes due to the injected carriers. So, the determination of $\bar{\kappa}_{\text{do}}$ provides vital information about the laser diode itself. This way of estimating $\bar{\kappa}_{\text{do}}$ can be used not only for bulk resonators but also for on-chip ones.

III. NEAR-IR EXPERIMENT

To verify the proposed technique, we perform some measurements of the FLR and BLR dependencies on the resonator-to-coupler gap (with the control of the Q factor at zero gap to determine the vertical index of the mode) for the MgF₂ microresonator at 1550 nm, and compare the calculated quality factor with the result obtained with the well-known ringdown method.

The WGMs are excited by a BK7 coupling prism with a distributed feedback (DFB) laser diode, with exact wavelength 1549.5 nm and power below 2 mW. The microresonator is 4 mm in diameter with 0.5 mm side curvature radius. The experimental setups and algorithm are presented in Fig. 1.

The translation stage with piezo element (PZT) was previously experimentally calibrated, and the measured displacement coefficient was $0.27 \pm 0.01 \mu\text{m/V}$. The step size of the PZT is 27 nm with our controller. We measure the dependence of the locking width on the piezo voltage (which gives the gap value) both when the frequency is increased and decreased. FLR + BLR is measured using a calibration interferometer with 93 MHz free spectral range. The calibration interferometer is made with a 90:10 beam splitter and mirrors. Observing the interference fringes, one may determine the frequency scale. The interferometer is continuously available, but during the measurements it is blocked to make the mode spectra clearer. For the locking width measurements, we use a detector with a large sensitive area of 19.6 mm² and 460 kHz bandwidth, and for the ringdown measurements, the detector area is 0.8 mm² and the bandwidth is 700 MHz. It is important that the locking phase does not change during the loading (see Fig. 3, in which the transmission resonance curves are presented). Every line is like an “isogap,” whose value one may find

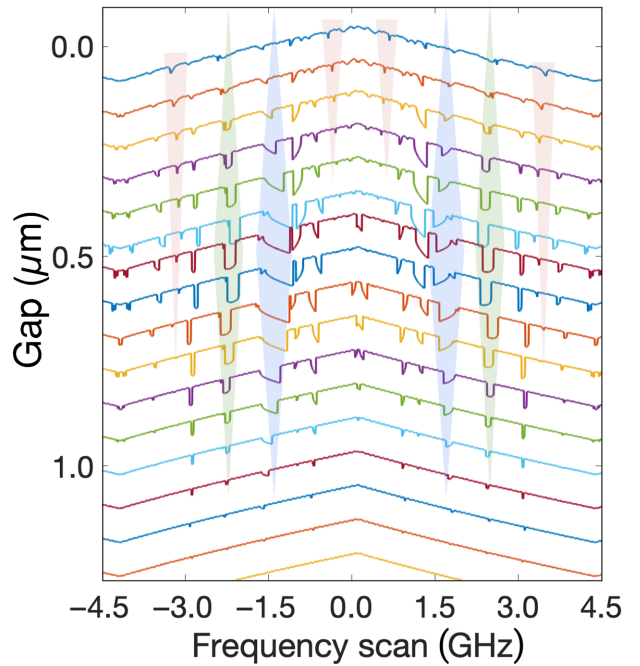


FIG. 3. LI curves measured for different gap values. The highlighted regions correspond to the excited modes with different polar indices: $p = 0$ (light green), $p = 2$ (light blue), and high p (light red). The mode shapes remain constant upon variation of the gap value, which indicates that the locking phase ψ_0 remains unchanged.

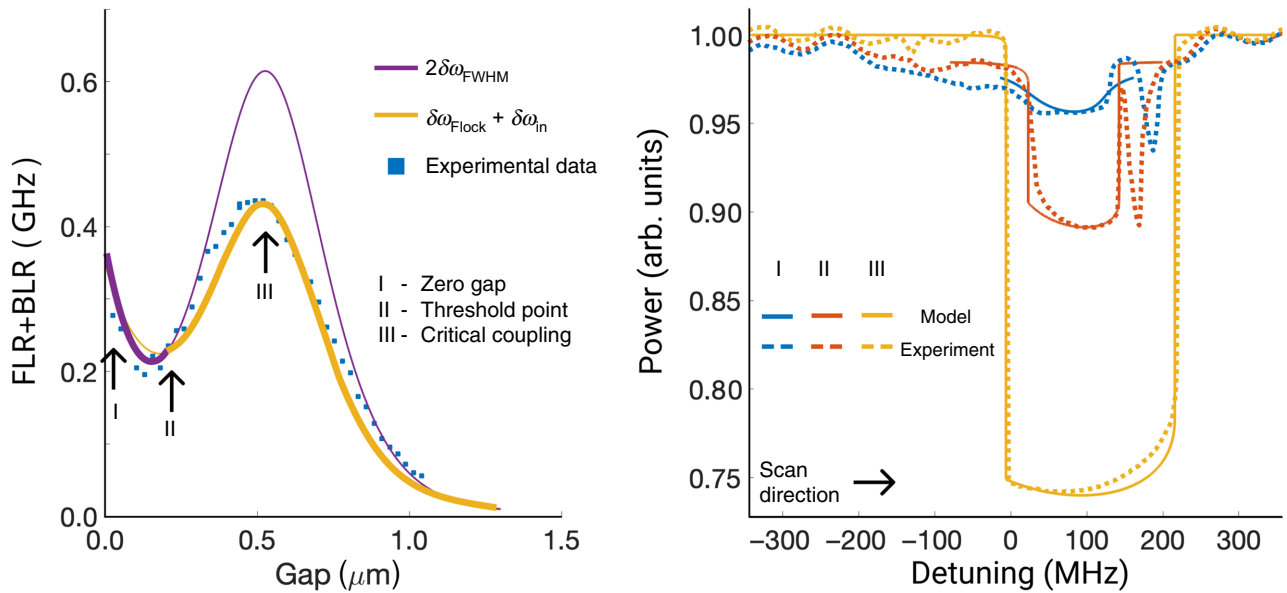


FIG. 4. Left panel: FLR + BLR dependence for the mode with $p = 0$. The transition to the “soft” regime occurs at a gap of around $0.2 \mu\text{m}$, and the fit with $\delta\omega_{\text{FWHM}}$ is valid for gap values less than $0.2 \mu\text{m}$. Right panel: mode traces at zero gap (I), the transition point (II; $\text{FLR} + \text{BLR} = 4\kappa_m$), and the critical coupling point (III; $\kappa_{mi} = \kappa_{mc}$). The experimental curves are plotted with dotted lines and the approximation curves generated using the linear SIL model are plotted with solid lines. The high-order mode appeared at overcoupling.

on the y axis. In the mode traces, the modes with different p and Q are distinguishable. The modes from different WGM families are excited, so different locking phases are observed on a trace. The colored areas in Fig. 3 correspond to different types of excited mode. The modes highlighted with red had high p and lower Q , so that they appeared closer to the coupler and remained narrow. The mode highlighted with green had $p = 0$ and $Q_{\text{int}} = 0.8 \times 10^8$, and its FLR + BLR dependence from the gap is shown in the left panel of Fig. 4. A critical coupling point (maximum) and transition point (“hard” to “soft” SIL) are respectively labeled III and II. There is a pronounced minimum in this case. It appears between the points where the FLR + BLR is wide due to self-injection locking and the overcoupled regime of the microresonator. At this point the LI curve becomes narrower, transforming to the “soft” regime while κ_c is not large yet. We also note that, while $\delta\omega_{\text{lock}} > \delta\omega_{\text{FWHM}}$ in the “hard” regime, $\delta\omega_{\text{lock}} + \delta\omega_{\text{in}} < 2\delta\omega_{\text{FWHM}}$ and vice versa for the soft regime. We compare the LI curves at the three mentioned points with a linear SIL model approximation [58] in the right panel of Fig. 4. First, we subtract the transmission inclination due to the laser diode power change during the frequency scan from experimental data and normalize the signal to the off-resonant power. We note that the experimental transmission in the critical coupling regime is 74% (see the dashed lines in the right panel of Fig. 4) instead of close to the zero value. This is due to imperfect mode matching in the experiment and the theoretical curves should be modified accordingly. The residual sinusoidal transmission oscillations refer to the

calibration interferometer. Then we calculate Q_m and Q_{int} for the mentioned points and experimentally measure $\bar{\kappa}_{\text{do}}$. Using this data as input parameters for the modeling, we carry out an approximation (see the solid lines in the right panel of Fig. 4) and get excellent agreement for the resonance curve form. The locking phase is initially assumed to be zero as forward and backward scans look symmetric (slight shift to $\pi/10$ makes the coincidence even better). However, after the alignment of mode III we had to further shift the positions of the theoretical curves for modes I and II to the right by 65 and 50 MHz for perfect matching. We attribute this to thermal effects, not included in the model, that increasingly shift the mode as a whole as the dip deepens (corresponding to the higher intracavity power). We also note that the power in the wide region near the mode drops slightly. This probably happens due to power leakage into some low- Q mode, revealed with loading. To account for this, we also lower the unity levels for theoretical curves I and II by 0.015 and 0.02. A mode from another family becomes visible in curves I and II to the right from the locked one during the coupling increase, while initially in III it is hidden by the locking. We also find that the mode shape near the coupler depends on $\bar{\kappa}_{\text{do}}$: the lower $\bar{\kappa}_{\text{do}}$, the closer the mode shape is to Lorentzian.

In many cases the transmission to the “soft” regime (without sharp edges) appears when the resonator is close enough to the coupler. It allows the direct determination of p by the linewidth at zero gap (see Table I). But in some cases, when the dimensionless coupling rate between counterpropagating modes and the vertical index of the

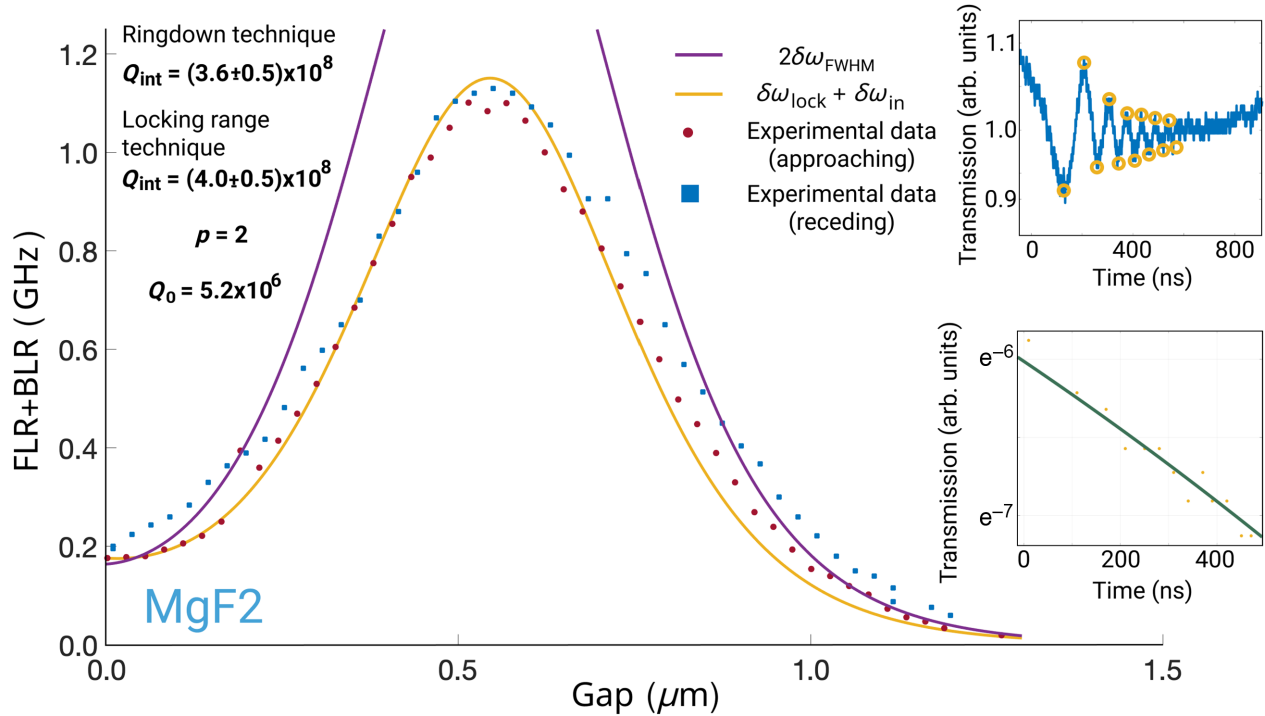


FIG. 5. Dependence of FLR + BLR on the gap for the MgF_2 microresonator. The experimental data is denoted using symbols, with the red circles representing an approaching microresonator and the blue squares representing a receding microresonator with respect to the coupler. The yellow solid line is the $\delta\omega_{lock} + \delta\omega_{in}$ curve calculated using Eqs. (1) and (2). The violet solid line is $2\delta\omega_{FWHM}$ calculated using Eq. (3). The extremum takes place at $550\ \mu m$, which gives $Q_{int} = (4.0 \pm 0.5) \times 10^8$ and $p = 2$. The ringdown method yields $Q_{int} = (3.6 \pm 0.5) \times 10^8$; see the insets.

mode are high enough, the SIL regime can be observed at zero gap. Once the microresonator reaches the surface of the coupler, the resonance remains constant.

The mode highlighted in blue in Fig. 3 had a locking phase near π . We changed its phase to zero by moving the laser and performed measurements of its FLR + BLR dependence on the gap value; see Fig. 5. Here the locking range is much wider and a transition from the “hard” to the “soft” regime is not easily noticeable. The extremum is at $d = 550\ \mu m$ from the coupler, which corresponds to an internal Q factor $Q_{int} = (4.0 \pm 0.5) \times 10^8$ for $p = 2$. One may see that FLR + BLR is a bit wider when the microresonator recedes from the coupler, which is caused by the hysteresis of the piezo element. It is worth noting that there is a strong dependence of the extremum location on p , when it changes from $p = 0$ to $p > 0$. This dependence is weak for the high p values, and for the q index also [69]. The transition point to the “hard” locking regime for modes with $p = 0$ is reached earlier than for $p > 0$; as κ_c increases faster, the combined coupling coefficient decreases to values not enough for the strong SIL.

Finally, we perform quality-factor measurements of the mode highlighted in blue in Fig. 3 via the ringdown method. We use an external narrow-linewidth fiber laser with an optical isolator. To excite the same WGM, we

determine its exact frequency by beating transmitted light with a laser with isolator at the undercoupled regime. Then, we fix the polarization with a Glan-Thompson prism. Finally, we adjust the power of the external laser with an isolator to make it equal to the DFB laser power. Thus, the mode is excited with the external laser with an isolator at the same frequency, the same polarization, and the same power. The WGM’s intrinsic quality factor is measured using the ringdown method in the undercoupled regime as $Q_{int} = (3.6 \pm 0.5) \times 10^8$. To verify that there is no degradation of Q_{int} during the measurements, we additionally check that the locking width does not change after these measurements.

To measure the backscattering, we add a 50:50 beam splitter between the coupling lens and the external laser with an isolator. Half of the backscattering is coupled to the photodetector, so we measure Γ_m^2 . From the previous experiments we can evaluate $\gamma\bar{\kappa}_{do}$ as a fit parameter. The backscattering wave measurements allows us to measure γ as a part of Γ_m separately from $\bar{\kappa}_{do}$. The measured reflected power for the critical coupling is $\frac{1}{150}$ part of the input power ($\Gamma_m^2 = \frac{1}{150}$). One may calculate $\bar{\kappa}_{do}/(2\pi) = 1.2 \times 10^{10}\ Hz$.

The Q factor measured with the proposed technique is in good agreement with the value measured via the

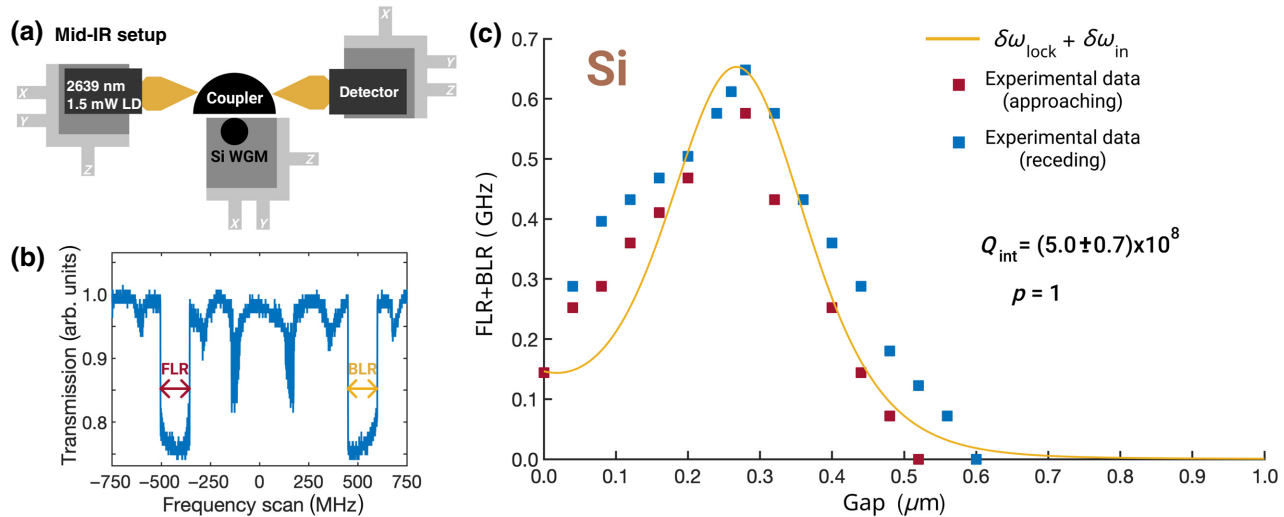


FIG. 6. (a) Experimental setup in the mid-IR. (b) Mode scan at critical coupling. (c) Dependence of FLR + BLR on the gap for the Si microresonator at 2639 nm. The blue and red squares represent the experimental data and the yellow solid line is calculated using Eq. (2). The extremum takes place at $270 \mu\text{m}$, giving $Q_{\text{int}} = 5.0 \times 10^8$ and $p = 1$.

conventional ringdown method, which confirms the applicability of the technique. The proposed technique provides a unique opportunity to accurately measure the Q factor via SIL without changing the setup or introducing additional equipment.

IV. MID-IR EXPERIMENT

The developed technique is applied to determine the Q factor of a silicon microresonator at 2639 nm. The microresonator made of crystalline silicon is polished according to the technique described in Ref. [30] to provide low surface losses. First, we determined the internal Q factor of this microresonator at 1550 nm as $(1-2) \times 10^8$ depending on the mode. The Q factor is measured using an external laser with an isolator by measuring the FWHM.

In the mid-IR experiment light is coupled to the microresonator by a hemisphere made of silicon. The temperature stabilized 2639 nm DFB diode laser is used as a pump laser. A temperature stabilized InAs photodiode with an amplifier that has a 10 MHz bandwidth and $100 \mu\text{W}$ saturation power is used as a detector. The immersive lens allowed us to couple a millimeter-scale beam to the detector. Measurements of the WGM's Q factor using the ringdown method are impossible here due to the absence of a detector with high bandwidth, and limitations to the laser sweep speed. We conducted the experiments with an attenuating plate between the laser and a coupler to suppress the backscattering (and SIL) to determine the Q factor by measuring the FWHM. Accurate measurements of the quality factor are impossible due to the thermo-optical oscillations and laser noise. However, we estimated the linewidth of the microresonator at zero gap

to be approximately 15 MHz, which corresponds to $p > 0$. The proposed technique provides us with a unique opportunity to determine the microresonator's parameters via self-injection locking. The thermo-optical oscillations are drastically suppressed in the SIL regime [see Fig. 6(b)]. The internal Q -factor value of the WGM microresonator is as high as $(5.0 \pm 0.7) \times 10^8$ and the vertical index of the mode $p = 1$ [see Fig. 6(c)].

At the zero gap there is a mode with sharp edges having a width of about 70 MHz. The significant increase in the Q factor in the mid-IR range compared to that in the near-IR range indicates that the main mechanism of losses is Rayleigh scattering. This confirms the assumption of attainability of ultra-high Q factors in silicon WGM microresonators in the mid-IR. The broadening of the locking range when the microresonator is receeded from the coupler caused by the hysteresis of the piezo element is also observed. The total locking range for small d is higher than theory predictions. We suppose that this is due to the thermal effects in silicon, which are particularly noticeable because the coupler and microresonator are both made of silicon, so the slightest changes in the refractive index are marked. This effect reduced, but did not vanish for decreasing incident power and for other modes. The total locking range exceeded 0.6 GHz, which for $Q_{\text{int}} = (5.0 \pm 0.7) \times 10^8$, corresponds to the stabilization coefficient $K = 16\delta\omega_{\text{lock}}/3\sqrt{3}\kappa_m = 4200$.

V. CONCLUSION

We develop, verify, and implement an original technique in an experiment that allows us to determine the parameters of the reference microcavity in the SIL regime. The

method is applicable for various spectral ranges, especially where it would be difficult to use established methods. The determination of the intrinsic Q factor is achieved by measuring the locking width evolution upon changing the gap between the coupler and microresonator. In contrast to the method based on resonance depth analysis [60], this technique allows for Q factor determination in the SIL regime, vertical mode index p identification, and is not susceptible to stray light entering the photodetector. Information on the p index of the mode increases the accuracy of the measurements. We experimentally show that the phase of SIL stays constant during variation of the gap between the microresonator and the coupler. Additionally measuring the backscattering, we determine the effective output beam coupling rate of the laser, which is a key parameter for modeling a SIL laser.

The technique is also used to determine the WGM's parameters of a silicon microcavity at 2639 nm. The elaborated approach allows us to determine an internal Q factor of the locking mode equal to $(5 \pm 0.7) \times 10^8$. Such a high value of the quality factor directly observed in silicon verifies the significant possibilities of silicon microresonators for mid-IR photonics.

ACKNOWLEDGMENTS

This work is supported by the Russian Science Foundation (Grant No. 20-12-00344). A.E.S. and V.E.L. acknowledge the Foundation for the Advancement of Theoretical Physics and Mathematics “BASIS” for personal support.

- [1] T. Ohta and K. Murakami, Reducing negative resistance oscillator noise by self-injection, *Electron. Commun. Jpn.* **51-B**, 80 (1968).
- [2] T. Ota and M. Nata, Noise reduction of oscillator by injection locking, *Trans. IECEJ* **53-B**, 487 (1970).
- [3] H.-C. Chang, Phase noise in self-injection-locked oscillators - theory and experiment, *IEEE Trans. Microw. Theory Tech.* **51**, 1994 (2003).
- [4] J. J. Choi and G. W. Choi, Experimental observation of frequency locking and noise reduction in a self-injection-locked magnetron, *IEEE Trans. Electron Devices* **54**, 3430 (2007).
- [5] M. Yu. Glyavin, G. G. Denisov, M. L. Kulygin, and Yu. V. Novozhilova, Stabilization of gyrotron frequency by reflection from nonresonant and resonant loads, *Tech. Phys. Lett.* **41**, 628 (2015).
- [6] L. Zhang, A. K. Poddar, U. L. Rohde, and A. S. Daryoush, Self-ILPLL using optical feedback for phase noise reduction in microwave oscillators, *IEEE Photonics Technol. Lett.* **27**, 624 (2015).
- [7] L. Zhang, A. K. Poddar, U. L. Rohde, and A. S. Daryoush, in *2015 IEEE 15th Topical Meeting on Silicon Monolithic Integrated Circuits in RF Systems* (IEEE, San Diego, CA, USA, 2015), p. 86.
- [8] V. L. Velichanskii, A. S. Zibrov, V. S. Kargopol'tsev, V. I. Molochev, V. V. Nikitin, V. A. Sautenkov, G. G. Kharisov, and D. A. Tyurikov, Minimum line width of an injection laser, *Sov. Tech. Phys. Lett. (Engl. Transl.)*; (United States) **4:9**, 438 (1978).
- [9] R. Lang and K. Kobayashi, External optical feedback effects on semiconductor injection laser properties, *IEEE J. Quantum Electron.* **16**, 347 (1980).
- [10] É. M. Belenov, V. L. Velichanskii, A. S. Zibrov, V. V. Nikitin, V. A. Sautenkov, and A. V. Uskov, Methods for narrowing the emission line of an injection laser, *Sov. J. Quantum Electron.* **13**, 792 (1983).
- [11] E. Patzak, H. Olesen, A. Sugimura, S. Saito, and T. Mukai, Spectral linewidth reduction in semiconductor lasers by an external cavity with weak optical feedback, *El. Lett.* **19**, 938 (1983).
- [12] G. Agrawal, Line narrowing in a single-mode injection laser due to external optical feedback, *IEEE J. Quantum Electron.* **20**, 468 (1984).
- [13] R. Tkach and A. Chraplyvy, Regimes of feedback effects in 1.5- μm distributed feedback lasers, *J. Lightwave Technol.* **4**, 1655 (1986).
- [14] B. Dahmani, L. Hollberg, and R. Drullinger, Frequency stabilization of semiconductor lasers by resonant optical feedback, *Opt. Lett.* **12**, 876 (1987).
- [15] L. Hollberg and M. Ohtsu, Modulatable narrow-linewidth semiconductor lasers, *Appl. Phys. Lett.* **53**, 944 (1988).
- [16] H. Li and N. B. Abraham, Analysis of the noise spectra of a laser diode with optical feedback from a high-finesse resonator, *IEEE J. Quantum Electron.* **25**, 1782 (1989).
- [17] A. Hemmerich, D. H. McIntyre, D. Schropp, D. Meschede, and T. W. Hänsch, Optically stabilized narrow linewidth semiconductor laser for high resolution spectroscopy, *Opt. Commun.* **75**, 118 (1990).
- [18] A. Hemmerich, C. Zimmermann, and T. W. Hänsch, Compact source of coherent blue light, *Appl. Opt.* **33**, 988 (1994).
- [19] D. R. Hjelme, A. R. Mickelson, and R. G. Beausoleil, Semiconductor laser stabilization by external optical feedback, *IEEE J. Quantum Electron.* **27**, 352 (1991).
- [20] V. B. Braginsky, M. L. Gorodetsky, and V. S. Ilchenko, Quality-factor and nonlinear properties of optical whispering-gallery modes, *Phys. Lett. A* **137**, 393 (1989).
- [21] A. A. Savchenkov, V. S. Ilchenko, A. B. Matsko, and L. Maleki, Kilohertz optical resonances in dielectric crystal cavities, *Phys. Rev. A* **70**, 051804(R) (2004).
- [22] A. B. Matsko and V. S. Ilchenko, Optical resonators with whispering-gallery modes-part I: Basics, *IEEE J. Sel. Top. Quantum Electron.* **12**, 3 (2006).
- [23] A. A. Savchenkov, A. B. Matsko, V. S. Ilchenko, and L. Maleki, Optical resonators with ten million finesse, *Opt. Express* **15**, 6768 (2007).
- [24] J. Ward and O. Benson, WGM microresonators: Sensing, lasing and fundamental optics with microspheres, *Laser Photonics Rev.* **5**, 553 (2011).
- [25] G. Lin, S. Diallo, R. Henriet, M. Jacquot, and Y. K. Chembo, Barium fluoride whispering-gallery-mode disk-resonator with one billion quality-factor, *Opt. Lett.* **39**, 6009 (2014).
- [26] R. Henriet, G. Lin, A. Coillet, M. Jacquot, L. Furfaro, L. Larger, and Y. K. Chembo, Kerr optical frequency comb

- generation in strontium fluoride whispering-gallery mode resonators with billion quality factor, *Opt. Lett.* **40**, 1567 (2015).
- [27] D. V. Strekalov, C. Marquardt, A. B. Matsko, H. G. L. Schwefel, and G. Leuchs, Nonlinear and quantum optics with whispering gallery resonators, *J. Opt.* **18**, 123002 (2016).
- [28] I. S. Grudinin, A. B. Matsko, A. A. Savchenkov, D. Strekalov, V. S. Ilchenko, and L. Maleki, Ultra high Q crystalline microcavities, *Opt. Commun.* **265**, 33 (2006).
- [29] C. Lecaplain, C. Javerzac-Galy, M. L. Gorodetsky, and T. J. Kippenberg, Mid-infrared ultra-high-Q resonators based on fluoride crystalline materials, *Nat. Commun.* **7**, 13383 (2016).
- [30] A. E. Shitikov, I. A. Bilenko, N. M. Kondratiev, V. E. Lobanov, A. Markosyan, and M. L. Gorodetsky, Billion Q -factor in silicon WGM resonators, *Optica* **5**, 1525 (2018).
- [31] M. L. Gorodetsky, A. D. Pryamikov, and V. S. Ilchenko, Rayleigh scattering in high-Q microspheres, *J. Opt. Soc. Am. B* **17**, 1051 (2000).
- [32] V. V. Vassiliev, V. L. Velichansky, V. S. Ilchenko, M. L. Gorodetsky, L. Hollberg, and A. V. Yarovitsky, Narrow-line-width diode laser with a high-Q microsphere resonator, *Opt. Commun.* **158**, 305 (1998).
- [33] V. V. Vassiliev, S. M. Il'ina, and V. L. Velichansky, Diode laser coupled to a high-Q microcavity via a GRIN lens, *Appl. Phys. B* **76**, 521 (2003).
- [34] W. Liang, V. S. Ilchenko, A. A. Savchenkov, A. B. Matsko, D. Seidel, and L. Maleki, Whispering-gallery-mode-resonator-based ultranarrow linewidth external-cavity semiconductor laser, *Opt. Lett.* **35**, 2822 (2010).
- [35] W. Liang, V. Ilchenko, A. A. Eliyahu, D. Savchenkov, A. B. Matsko, and D. Seidel, Ultralow noise miniature external cavity semiconductor laser, *Nat. Commun.* **6**, 7371 (2015).
- [36] E. Dale, M. Bagheri, A. B. Matsko, C. Frez, W. Liang, S. Forouhar, and L. Maleki, Microresonator stabilized 2 μm distributed-feedback GaSb-based diode laser, *Opt. Lett.* **41**, 5559 (2016).
- [37] A. A. Savchenkov, D. Eliyahu, B. Heist, A. B. Matsko, M. Bagheri, C. Frez, and S. Forouhar, On acceleration sensitivity of 2 μm whispering gallery mode-based semiconductor self-injection locked laser, *Appl. Opt.* **58**, 2138 (2019).
- [38] P. S. Donvalkar, A. Savchenkov, and A. Matsko, Self-injection locked blue laser, *J. Opt.* **20**, 045801 (2018).
- [39] R. R. Galiev, N. G. Pavlov, N. M. Kondratiev, S. Koptyaev, V. E. Lobanov, A. S. Voloshin, A. S. Gorodnitskiy, and M. L. Gorodetsky, Spectrum collapse, narrow linewidth, and bogatov effect in diode lasers locked to high-Q optical microresonators, *Opt. Express* **26**, 30509 (2018).
- [40] N. G. Pavlov, S. Koptyaev, G. V. Lihachev, A. S. Voloshin, A. S. Gorodnitskiy, M. V. Ryabko, S. V. Polonsky, and M. L. Gorodetsky, Narrow-linewidth lasing and soliton Kerr microcombs with ordinary laser diodes, *Nat. Photonics* **12**, 694 (2018).
- [41] Anatoliy A. Savchenkov, Sheng-Wey Chiow, Mohammadreza Ghasemkhani, Skip Williams, Nan Yu, Robert C. Stirbl, and Andrey B. Matsko, Self-injection locking efficiency of a UV fabry-perot laser diode, *Opt. Lett.* **44**, 4175 (2019).
- [42] A. S. Raja, A. S. Voloshin, H. Guo, S. E. Agafonova, J. Liu, A. S. Gorodnitskiy, M. Karpov, N. G. Pavlov, E. Lucas, R. Galiev, A. E. Shitikov, J. D. Jost, M. L. Gorodetsky, and T. J. Kippenberg, Electrically pumped photonic integrated soliton microcomb, *Nat. Commun.* **10**, 680 (2019).
- [43] Sylvain Boust, Houssein El Dirani, François Duport, Laurene Youssef, Yannick Robert, Alexandre Larrue, Camille Petit-Etienne, Eric Vinet, Sébastien Kerdiles, and Erwine Parfon *et al.*, in *2019 International Topical Meeting on Microwave Photonics (MWP)* (IEEE, Ottawa, Canada, 2019), p. 1.
- [44] T. C. Briles, J. R. Stone, S. B. Papp, G. Moille, K. Srinivasan, L. Chang, C. Xiang, J. Guo, and J. E. Bowers, in *2019 IEEE Avionics and Vehicle Fiber-Optics and Photonics Conference (AVFOP)* (IEEE, Arlington, Virginia, 2019), p. 1.
- [45] B. Shen, L. Chang, J. Liu, H. Wang, Q.-F. Yang, C. Xiang, R. N. Wang, J. He, T. Liu, W. Xie, J. Guo, D. Kinghorn, L. Wu, Q.-X. Ji, T. J. Kippenberg, K. Vahala, and J. E. Bowers, Integrated turnkey soliton microcombs, *Nature* **582**, 365 (2020).
- [46] A. S. Voloshin, N. M. Kondratiev, G. V. Lihachev, J. Liu, V. E. Lobanov, N. Yu. Dmitriev, W. Weng, T. J. Kippenberg, and I. A. Bilenko, Dynamics of soliton self-injection locking in a photonic chip-based microresonator, arXiv preprint [arXiv:1912.11303](https://arxiv.org/abs/1912.11303) (2020).
- [47] P. Marin-Palomo, J. N. Kemal, M. Karpov, A. Kordts, J. Pfeifle, M. H. P. Pfeiffer, P. Trocha, S. Wolf, V. Brasch, M. H. Anderson, R. Rosenberger, K. Vijayan, W. Freude, T. J. Kippenberg, and C. Koos, Microresonator-based solitons for massively parallel coherent optical communications, *Nature* **546**, 274 (2017).
- [48] A. Fülöp, M. Mazur, A. Lorences-Riesgo, Ó.B. Helgason, P.-H. Wang, Y. Xuan, D. E. Leaird, M. Qi, P. A. Andrekson, and A. M. Weiner *et al.*, High-order coherent communications using mode-locked dark-pulse Kerr combs from microresonators, *Nat. Commun.* **9**, 1598 (2018).
- [49] M.-G. Suh and K. J. Vahala, Soliton microcomb range measurement, *Science* **359**, 884 (2018).
- [50] P. Trocha, M. Karpov, D. Ganin, M. H. P. Pfeiffer, A. Kordts, S. Wolf, J. Krockenberger, P. Marin-Palomo, C. Weimann, S. Randel, W. Freude, T. J. Kippenberg, and C. Koos, Ultrafast optical ranging using microresonator soliton frequency combs, *Science* **359**, 887 (2018).
- [51] J. Riemensberger, A. Lukashchuk, M. Karpov, W. Weng, E. Lucas, J. Liu, and T. J. Kippenberg, Massively parallel coherent laser ranging using a soliton microcomb, *Nature* **581**, 164 (2020).
- [52] M.-G. Suh, Q.-F. Yang, K. Y. Yang, X. Yi, and K. J. Vahala, Microresonator soliton dual-comb spectroscopy, *Science* **354**, 600 (2016).
- [53] Q.-F. Yang, B. Shen, H. Wang, M. Tran, Z. Zhang, K. Y. Yang, L. Wu, C. Bao, J. Bowers, A. Yariv, and K. Vahala, Vernier spectrometer using counterpropagating soliton microcombs, *Science* **363**, 965 (2019).
- [54] E. Obrzud, M. Rainer, A. Harutyunyan, M. H. Anderson, J. Liu, M. Geiselmann, B. Chazelas, S. Kundermann, S. Lecomte, M. Cecconi, A. Ghedina, E. Molinari, F. Pepe, F. Wildi, F. Bouchy, T. J. Kippenberg, and T. Herr, A microphotonic astrocomb, *Nat. Photonics* **13**, 31 (2019).
- [55] M.-G. Suh, X. Yi, Y.-H. Lai, S. Leifer, I. S. Grudinin, G. Vasisht, E. C. Martin, M. P. Fitzgerald, G. Doppmann, J. Wang, D. Mawet, S. B. Papp, S. A. Diddams,

- C. Beichman, and K. Vahala, Searching for exoplanets using a microresonator astrocomb, *Nat. Photonics* **13**, 25 (2019).
- [56] S. B. Papp, K. Beha, P. Del'Haye, F. Quinlan, H. Lee, K. J. Vahala, and S. A. Diddams, Microresonator frequency comb optical clock, *Optica* **1**, 10 (2014).
- [57] Z. L. Newman *et al.*, Architecture for the photonic integration of an optical atomic clock, *Optica* **6**, 680 (2019).
- [58] N. M. Kondratiev, V. E. Lobanov, A. V. Cherenkov, A. S. Voloshin, N. G. Pavlov, S. Koptyaev, and M. L. Gorodetsky, Self-injection locking of a laser diode to a high-Q WGM microresonator, *Opt. Express* **25**, 28167 (2017).
- [59] T. J. Kippenberg, A. L. Gaeta, M. Lipson, and M. L. Gorodetsky, Dissipative Kerr solitons in optical microresonators, *Science* **361**, eaan8083 (2018).
- [60] A. A. Savchenkov, S. Borri, M. Siciliani de Cumis, A. Matsko, P. De Natale, and L. Maleki, Modeling and measuring the quality factor of whispering gallery mode resonators, *Appl. Phys. B* **124**, 171 (2018).
- [61] S. K. Tokunaga, C. Stoeffler, F. Auguste, A. Shelkovnikov, C. Daussy, A. e Amy-Klein, C. Chardonnet, and B. Darquié, Probing weak force-induced parity violation by high-resolution mid-infrared molecular spectroscopy, *Mol. Phys.* **111**, 2363 (2013).
- [62] J. Xia, F. Zhu, A. A. Kolomenskii, J. Bounds, S. Zhang, M. Amani, L. J. Fernyough, and H. A. Schuessler, Sensitive acetone detection with a mid-IR interband cascade laser and wavelength modulation spectroscopy, *OSA Continuum* **2**, 640 (2019).
- [63] S. Mejri, P. L. T. Sow, O. Kozlova, C. Ayari, S. K. Tokunaga, C. Chardonnet, S. Briaudeau, B. Darquié, F. Rohart, and C. Daussy, Measuring the Boltzmann constant by mid-infrared laser spectroscopy of ammonia, *Metrologia* **52**, S314 (2015).
- [64] Q. Hao, G. Zhu, S. Yang, K. Yang, T. Duan, X. Xie, K. Huang, and H. Zeng, Mid-infrared transmitter and receiver modules for free-space optical communication, *Appl. opt.* **56**, 2260 (2017).
- [65] H. Al-Taiy, N. Wenzel, S. Preußler, J. Klinger, and T. Schneider, Ultra-narrow linewidth, stable and tunable laser source for optical communication systems and spectroscopy, *Opt. Lett.* **39**, 5826 (2014).
- [66] A. D. Bristow, N. Rotenberg, and H. M. Van Driel, Two-photon absorption and Kerr coefficients of silicon for 850–2200 nm, *Appl. Phys. Lett.* **90**, 191104 (2007).
- [67] M. Hass and B. Bendow, Residual absorption in infrared materials, *Appl. Opt.* **16**, 2882 (1977).
- [68] R. R. Galiev, N. M. Kondratiev, V. E. Lobanov, A. B. Matsko, and I. A. Bilenko, Optimization of Laser Stabilization via Self-Injection Locking to a Whispering-Gallery-Mode Microresonator, *Phys. Rev. Appl.* **14**, 014036 (2020).
- [69] M. L. Gorodetsky and V. S. Ilchenko, High-Q optical whispering-gallery microresonators: Precession approach for spherical mode analysis and emission patterns with prism couplers, *Opt. Commun.* **113**, 133 (1994).